Description of collective and quasiparticle excitations in deformed actinide nuclei: The first application of the multishell shell model for heavy nuclei

Ji-Wei Cui,[1] Xian-Rong Zhou,[1,*] Fang-Qi Chen,[2] Yang Sun,[2] Cheng-Li Wu,[1] and Zao-Chun Gao[3]

[1]*Department of Physics and Institute of Theoretical Physics and Astrophysics, Xiamen University, Xiamen 361005, People's Republic of China*

[2]*Department of Physics and Astronomy, Shanghai Jiao Tong University, Shanghai 200240, People's Republic of China*

[3]*China Institute of Atomic Energy, P.O. Box 275(18), Beijing 102413, People's Republic of China*

(Received 24 March 2014; published 28 July 2014)

The heavy shell model (HSM) [Y. Sun and C.-L. Wu, Phys. Rev. C **68**, 024315 (2003)] was proposed to take the advantages of two existing models, the projected shell model (PSM) and the fermion dynamical symmetry model (FDSM). To construct the HSM, one extends the PSM by adding collective D pairs into the intrinsic basis. The HSM is expected to describe simultaneously low-lying collective and quasiparticle excitations in deformed nuclei, and still keeps the model space tractable even for the heaviest systems. As the first numerical realization of the HSM, we study systematically the band structures for some deformed actinide nuclei, with a model space including up to 4-quasiparticle and 1-D-pair configurations. The calculated energy levels for the ground-state bands, the collective bands such as β and γ bands, and some quasiparticle bands agree well with known experimental data. Some low-lying quasiparticle bands are predicted, awaiting experimental confirmation.

DOI: 10.1103/PhysRevC.90.014321 PACS number(s): 21.10.Re, 21.60.Cs, 23.20.Lv

I. INTRODUCTION

The interplay between collective motion and quasiparticle excitations has been a long-standing topic in nuclear structure physics. It is difficult to use the conventional shell model based on a spherical basis to study heavy, deformed nuclei because of the problem of huge dimensionality. Even with today's computer power and novel diagonalization algorithms, a full shell model calculation for an arbitrarily large system seems to be impossible. To overcome the dimensionality problem, one needs to seek judicious truncation schemes and use more efficient shell-model bases. In the literatures, the projected shell model (PSM) [1] and the fermion dynamical symmetry model (FDSM) [2] are two such examples. Both of them are based on the shell model concept, but are constructed according to different truncation schemes, thus emphasizing different physical aspects. It should be mentioned that Schmid and collaborators have provided another example (the MONSTOR-VAMPIR hierarchy) of truncation schemes based on the symmetry-restoration method. It offers approaches to describe rotational states with fully optimized symmetry-projected mean fields and more sophisticated effective interactions [3].

In the PSM, shell model diagonalization is carried out in the projected deformed basis constructed by choosing a few quasiparticle (qp) orbitals near the Fermi surfaces and performing angular-momentum and particle-number projection on the qp configurations [1]. In this way, the PSM is able to describe low-lying rotational bands built upon qp excitations. The PSM has been successful for studying the rotational states in heavy [4] and superheavy nuclei [5], as well as the states of superdeformation [6,7]. Moreover, it has been shown that, comparing with large-scale shell model calculations [8], the PSM can achieve a similar accuracy in describing the deformed ^{48}Cr [9] and the superdeformed ^{36}Ar [10]. However, the original version of the PSM was not designed to treat collective vibrational states such as β and γ vibrations. The lack of ingredients for collective excitations in the PSM makes it difficult to produce these low-lying collective bands, and also limits its applications only to well deformed nuclei. To release the restriction of axial symmetry in the deformed basis, the triaxial projected shell model (TPSM) was introduced [11]. A more recent example of the TPSM application is to describe the γ-vibrational bands in some Er isotopes [12].

On the other hand, the interacting boson model (IBM) [13] is a successful model for the description of low-lying collective states. In this model, the coherent S and D pairs are assumed to be the building blocks of the low-lying collective states, and are approximated as s and d bosons. It has been shown that an axially symmetric rotor possesses SU(3) symmetry, while a γ-soft rotor possesses SO(6) symmetry. The β and γ vibrations including the scissors mode vibration in deformed nuclei can be classified as different SU(3) or SO(6) irreducible representations [14]. Since nucleons are fermions, the later developed FDSM directly uses coherent nucleon S and D pairs without a boson approximation. The FDSM actually uses a symmetry-dedicated shell model truncation scheme to treat nuclear collective excitations. It has been shown that the FDSM can well describe the low-lying collective states from the spherical to the well-deformed region [2]. However, the FDSM has difficulties in describing single-particle excitations, because once the unpaired single-particle degrees of freedom are opened up, the dimension of the model space will go up quickly just as in the conventional spherical shell model. Moreover, the FDSM is a one-major-shell shell model.

It is clear that both the PSM and the FDSM follow the shell model philosophy, but they employ different truncation schemes, thus describing different excitation modes. The PSM emphasizes qp excitations, while the FDSM emphasizes low-lying collective excitations. Experimentally, it is often the case that quasiparticle and collective excitations coexist in the low-lying nuclear spectrum. It is therefore desired to

*Corresponding author: xrzhou@xmu.edu.cn

combine the advantages of these two models to form a new shell model for heavy nuclei, which can describe both qp excitations and low-lying collective excitations simultaneously. The combination of the two models becomes possible through the recognition [15,16] that the PSM calculations exhibit, up to high angular momenta and excitation energies, a remarkable one-to-one correspondence with the analytical SU(3) spectrum of the FDSM. Motivated by this finding, it was suggested in Ref. [17] that it is possible to treat collective and qp excitations in a common multishell shell-model framework. One way to realize the idea is to extend the PSM by adding the coherent D pairs into the intrinsic basis, since it is evident from the FDSM that it is the coherent D pairs that are responsible for the collective excitations. With this extension, the PSM (i.e., the HSM) may become a more general multi-major-shell shell model, useful not only for well deformed nuclei, but hopefully also for transitional ones (see discussions in Ref. [17]).

The key question for implementing the HSM is how to construct the D pairs in the PSM model space, which usually involves three major shells for both neutrons and protons. In Ref. [18], the D_0 (D_2) pair was suggested to be the linear combination of all the 2-qp states with $K^\pi = 0^+(K^\pi = 2^+)$ in the PSM multi-major-shell truncated space. The structure amplitudes are obtained from the wave function of the lowest 2-qp state after diagonalization. A testing calculation was performed for the β band in ^{172}Yb, and it was found that, indeed, the collective nature of the D_0 configuration can be well reproduced from the calculation [18]. In Ref. [19], it was shown that, by including both qp and D_0 configurations, the ground-state bands (g.s. bands) and β bands of four deformed nuclei, ^{230,232}Th and ^{232,234}U in the actinide region, are also well reproduced. In addition, the calculated $B(E2)$ transition rates agree well with the experimental data. The structure of the D_0 pair in the calculation does show collectivity. It is indeed a strong mixture of many 2-qp states. All these indicate that the suggested construction [18] of D_0 pair is reasonable.

The above attempts may be regarded as an initial step of the numeric realization of the HSM. However, in order to describe γ bands, one needs to add the D_2 pair into the PSM basis. Furthermore, in order to have the so-called "2-phonon states" one needs to consider 2-D-pair excitations. As suggested by the FDSM, the 2-D-pair excitations have four different excitation modes: D_0D_0, D_2D_0, D_2D_{-2}, and D_2D_2, which will give rise to the following four 2-phonon-excitation bands: $\beta\beta$ band ($n_\gamma = 0, n_\beta = 2, K/2 = 0$), $\gamma\beta$ band ($n_\gamma = 0$, $n_\beta = 1$, $K/2 = 1$), $\gamma\gamma(0^+)$ band ($n_\gamma = 2, n_\beta = 0, K/2 = 0$), and $\gamma\gamma(4^+)$ band ($n_\gamma = 0$, $n_\beta = 0$, $K/2 = 2$), respectively, where n_β, n_γ, and K denote the quantum numbers of β and γ phonons and the z component of angular momentum.

In Refs. [20,21], the rotational bands in the nuclei with $Z = 100$ were investigated systematically by using the cranking shell model with the pairing correlations treated by a particle-number conserving method. In the present paper, we study systemically the band structure of both the low-lying qp and collective excitations for the deformed actinide nuclei ^{230,232}Th, ^{232,234,236}U, and ^{240}Pu by adding 1-D pairs into the PSM basis.

This paper is organized as follows. A brief introduction of HSM is given in Sec. II. In Sec. III, we discuss in detail the structure of D_0 and D_2 pairs, the energy schemes, eigenfunctions, and reduced $B(E2)$ transitions for the nuclei ^{230,232}Th, ^{232,234,236}U, and ^{240}Pu, respectively. Finally, a conclusion is drawn in Sec. IV.

II. FORMULISM

The HSM is an improved version of PSM including not only single-particle excitations but also collective excitations in the basis. However, the PSM cannot use directly the D pair defined in the FDSM, since the two model spaces are very different. The structure of D pairs is suggested in Ref. [18] as follows:

$$D_0^\dagger = \sum_{\rho,\mu} f_{\rho\mu}^{K=0}[a_\rho^\dagger a_\mu^\dagger]^{K=0}, \quad D_2^\dagger = \sum_{\rho,\mu} f_{\rho\mu}^{K=2}[a_\rho^\dagger a_\mu^\dagger]^{K=2}, \tag{1}$$

where $[a_\rho^\dagger a_\mu^\dagger]^K$ is the 2-qp creation operator with $K = 0,2$. ρ and μ are the state index of the qp, and $f_{\rho\mu}^K$ is the structure amplitude, which are determined by diagonalizing the Hamiltonian in the 2-qp basis with given K. Having $D_0^\dagger$ and $D_2^\dagger$ determined, the 1-D-pair excitation will give the first β and γ bands. They can be expressed as

$$|I,M\rangle_\beta = \hat{P}_{M0}^I D_0^\dagger|\Phi\rangle, \quad |I,M\rangle_\gamma = \hat{P}_{M2}^I D_2^\dagger|\Phi\rangle, \tag{2}$$

where $|\Phi\rangle$ is the BCS vacuum and

$$\hat{P}_{MK}^I = \frac{2I+1}{8\pi^2}\int d\Omega\, \hat{D}_{MK}^I \hat{R}(\Omega) \tag{3}$$

is the angular momentum projection operator. In Eq. (3), D_{MK}^I is the irreducible representation of the rotation group and $\hat{R}$ is the rotation operator with respect to the solid angle Ω that is always denoted by three Euler angles (α, β, γ). In our calculation, the axial symmetry in the deformed basis is assumed, so the D function reduces to the d function and Ω reduces to β. Finally, adding the collective excitations into the PSM intrinsic basis, the HSM intrinsic basis is given. For even-even nuclei it is

$$\{|\phi_\kappa\rangle\} = \{|\Phi\rangle, a_{\nu_i}^\dagger a_{\nu_j}^\dagger|\Phi\rangle, a_{\pi_k}^\dagger a_{\pi_l}^\dagger|\Phi\rangle, a_{\nu_i}^\dagger a_{\nu_j}^\dagger a_{\pi_k}^\dagger a_{\pi_l}^\dagger|\Phi\rangle, D_0^\dagger|\Phi\rangle, D_2^\dagger|\Phi\rangle\}, \tag{4}$$

where $a_{\nu_i}^\dagger$ and $a_{\pi_i}^\dagger$ are the qp creation operators for neutrons and protons with i as state index, respectively. Configurations that contain more than two like-nucleon quasiparticles are not included, because they have higher excitation energies due to mutual blocking of levels and thus affect the results little in energy ranges that interest us [1]. Therefore, the 4-qp configurations in (4) have a particular form that consists of two-proton and two-neutron operators only. They are expected to play the most important role in the 4-qp excitations.

It should be stressed that the HSM truncation is carried out in the intrinsic basis (a symmetry-breaking deformed mean-field basis that has already contained much of the multishell correlations due to the nuclear deformations), and then subsequently the rotational symmetry is recovered via the projection operator. The combination of these two is what makes this kind of approache a very powerful truncation

scheme, which is at variance with the traditional shell model where the truncation is based on a spherical mean-field basis and is unsuitable for handling multi-major-shell correlations. Here, as also discussed in Ref. [3], an efficient truncation is achieved by transferring the truncation hierarchy to a highly correlated symmetry-projected basis where each state is a significant mixing of multiple major shells.

The shell-model configuration space can then be constructed by the projected basis, which is

$$|K,\kappa,IM\rangle = \hat{P}^I_{MK}|\phi_\kappa\rangle, \tag{5}$$

where $|\phi_\kappa\rangle$ denotes the intrinsic basis of HSM given in Eq. (4). Then we can obtain the eigenenergy E^σ and the eigen wave function

$$\left|\Psi^{I,\sigma}_M\right\rangle = \sum_{K,\kappa} F^{I,\sigma}_{K,\kappa}|K,\kappa,IM\rangle, \tag{6}$$

where σ denotes different eigenstates, by solving the following eigenvalue equation:

$$\sum_{K',\kappa'}\left(\hat{H}^I_{K\kappa,K'\kappa'} - E^\sigma \hat{N}^I_{K\kappa,K'\kappa'}\right)F^{I\sigma}_{K'\kappa'} = 0, \tag{7}$$

where the Hamiltonian matrix element and the norm matrix element are

$$\hat{H}^I_{K\kappa,K'\kappa'} = \langle\phi_\kappa|\hat{H}\hat{P}^I_{KK'}|\phi_{\kappa'}\rangle, \tag{8}$$

$$\hat{N}^I_{K\kappa,K'\kappa'} = \langle\phi_\kappa|\hat{P}^I_{KK'}|\phi_{\kappa'}\rangle. \tag{9}$$

The effective interaction employed in the HSM is the same as that in the PSM, which takes the form

$$\hat{H} = \sum_{\xi=\nu,\pi}\hat{H}_\xi + \hat{H}_{\nu\pi}, \quad \hat{H}_{\nu\pi} = -\chi_{\nu\pi}\hat{Q}^{\nu\dagger}_2\hat{Q}^\pi_2,$$
$$\hat{H}_\xi = \hat{H}^\xi_0 - \frac{\chi_\xi}{2}\hat{Q}^{\xi\dagger}_2\hat{Q}^\xi_2 - G^\xi_M\hat{P}^{\xi\dagger}\hat{P}^\xi - G^\xi_Q\hat{P}^{\xi\dagger}_2\hat{P}^\xi_2. \tag{10}$$

The first term $\hat{H}^\xi_0$ in Eq. (10) is the spherical single-particle Hamiltonian. The second term is the residual quadrupole-quadrupole interaction, while the third and fourth terms are the monopole-pairing and quadrupole-pairing interactions, respectively. The strength of the quadrupole-quadrupole force is related to the quadrupole deformation in the Nilsson potential by [1,22]

$$\chi_{\tau\tau'} = \frac{\frac{2}{3}\epsilon_2\hbar\omega_\tau\hbar\omega_{\tau'}}{\hbar\omega_\nu\langle Q_0\rangle_\nu + \hbar\omega_\pi\langle Q_0\rangle_\pi}, \tag{11}$$

where τ and τ' mean either ν or π. The monopole-pairing strength is given as follows:

$$G^n_M = (19.3 - 0.08(N-Z))/A,$$
$$G^p_M = (13.3 + 0.217(N-Z))/A, \tag{12}$$

where n denotes neutrons and p denotes protons. The monopole-pairing strength above is determined by reproducing the experimental odd-even mass difference as Ref. [23]. In the current calculation it is multiplied by 0.87 in the cases of both neutrons and protons. The quadrupole-pairing strength G_Q is proportional to G_M and the proportional rate G_Q/G_M is fixed to 0.14 in our calculation for ^{230,232}Th, 0.13 for ^{232,234,236}U, and 0.12 for ^{240}Pu. The parameters we choose are slightly different from Refs. [19] and [24,25] due to the different spaces used in our present model. In FDSM, to produce the SU(3) symmetry, the quadrupole-pairing strength is equal to the monopole-pairing strength [2]. The origin of the difference remains a very interesting topic.

In Eq. (10), the one-body operator takes the following form:

$$\hat{Q}_\mu = \sum_{\alpha,\alpha'} Q_{\mu\alpha\alpha'}c^\dagger_\alpha c_{\alpha'},$$
$$\hat{P}^\dagger = \frac{1}{2}\sum_\alpha c^\dagger_\alpha c^\dagger_{\bar{\alpha}},$$
$$\hat{P}^\dagger_\mu = \frac{1}{2}\sum_{\alpha,\alpha'} Q_{\mu\alpha\alpha'}c^\dagger_\alpha c^\dagger_{\bar{\alpha'}}. \tag{13}$$

In the above equations, $Q_{\mu\alpha\alpha'}$ is the matrix element of the one-body quadrupole operator, namely $\langle\alpha|\hat{Q}_{2\mu}|\alpha'\rangle$ in which α represents the spherical single-particle state denoted by $\{nljm\}$. $c^\dagger_\alpha$ is the particle creation operator on the corresponding state and its time reversal is defined as $c_{\bar{\alpha}} = (-1)^{j-m}c_{nlj-m}$.

When the eigenvalue equation [Eq. (7)] is solved, the eigenstates can be determined. Correspondingly, the electric quadrupole transition probabilities between the states $|\Psi^{I\sigma}\rangle$ and $|\Psi^{I'\sigma'}\rangle$ can be calculated by the quadrupole operator [Eq. (13)]:

$$B(E2, I\sigma \to I'\sigma') = \frac{2I'+1}{2I+1}|\langle\Psi^{I'\sigma'}\|\hat{Q}_2\|\Psi^{I\sigma}\rangle|^2, \tag{14}$$

where the reduced matrix element is defined as

$$\langle\Psi^{I'\sigma'}\|\hat{Q}_2\|\Psi^{I\sigma}\rangle = \sum_{KK',\kappa\kappa',\nu}(IK' - \nu,2\nu|I'K')$$
$$\times\langle\Phi_{\kappa'}|\hat{Q}_{2\nu}\hat{P}^I_{K'-\nu,K}|\Phi_\kappa\rangle F^{I'\sigma'}_{K'\kappa'}F^{I\sigma}_{K\kappa}. \tag{15}$$

An effective charge of $0.5e$ is used to compute the $B(E2)$ values.

III. RESULTS

In the calculation, Nilsson's parameters (κ, μ) for ^{230,232}Th, ^{232,234,236}U, and ^{240}Pu are taken from Refs. [26,27], and the shapes of the Nilsson's deformed field for each nucleus are fixed. They are described by ϵ_2 and ϵ_4 for quadrupole and hexadecapole deformations which are listed in Table I. The ϵ_2 value (bear in mind that the relation between ϵ_2 and β_2 is approximately $\epsilon_2 = \beta_2 \times 0.95$) is fixed for each nucleus

TABLE I. The quadrupole and hexadecapole deformation parameters for ^{230,232}Th, ^{232,234,236}U, and ^{240}Pu, respectively.

	^{230}Th	^{232}Th	^{232}U	^{234}U	^{236}U	^{240}Pu
ϵ_2	0.212	0.234	0.238	0.240	0.254	0.260
ϵ_4	0.013	0.018	0.012	0.027	0.030	0.040

TABLE II. The chemical potentials of neutron and proton for ^{230,232}Th, ^{232,234,236}U, and ^{240}Pu. The unit is MeV.

	^{230}Th	^{232}Th	^{232}U	^{234}U	^{236}U	^{240}Pu
λ_n	53.42	53.69	53.20	53.38	53.52	53.21
λ_p	39.76	39.49	39.97	39.76	39.54	39.54

changing from 0.212 to 0.260. We see from Table I that the ε_2 values of quadrupole deformations increase as the numbers of valence nucleons increase. They are approximately in accordance with the results of nonrelativistic mean-field calculation with the Gogny force [28] and the relativistic mean-field (RMF) calculation [29]. Meanwhile, the hexadecapole deformation parameter ϵ_4 is nearly one order smaller than ϵ_2.

Particle number is conserved at the BCS level. In the present model, the right average particle number is obtained by adding the term $-\lambda\hat{N}$ to the Hamiltonian

$$H' = H - \lambda\hat{N}, \tag{16}$$

where the Lagrange multiplier λ is fixed by the condition [30]

$$\langle \mathrm{BCS}|\hat{N}|\mathrm{BCS}\rangle = 2\sum_k v_k^2 = N. \tag{17}$$

In Table II, we list the obtained Lagrange multipliers for all nuclei studied in the present paper.

The difference between the current HSM and PSM is that the collective excitations described by the D_0 and D_2 pair are included in the basis space [see Eq. (4)]. The first thing we need to check is the collectivity of the D_0 and D_2 pair. In the single-particle space (three major shells, $N = 4,5,6$ for protons and $N = 5,6,7$ for neutrons), the numbers of $K = 0$ and $K = 2$ 2-qp states are about 60 and 80, respectively, in the case of truncation energy 5 MeV. The main components (percentages are larger than 2%) of the D_0 and D_2 pair are listed in Tables III and IV for ^{232,234}Th, $^{232-236}$U, and ^{240}Pu, respectively.

In Table III, we notice that for neutron configurations, except the 2-qp state $\frac{5}{2}^+[633]_\nu - \frac{5}{2}^+[622]_\nu$, all the others are composed of one qp state and its time reversal partner. The basis $\frac{1}{2}^+[631]_\nu - \frac{1}{2}^+[631]_\nu$ plays an important role for all the nuclei studied. On the other hand, for all the nuclei except

TABLE III. The main configurations of the D_0 pairs constructed as in Eq. (1) for ^{230,232}Th, ^{232,234,236}U, and ^{240}Pu, respectively.

2-qp basis	^{230}Th	^{232}Th	^{232}U	^{234}U	^{236}U	^{240}Pu
$\frac{5}{2}^-[503]_\nu - \frac{5}{2}^-[503]_\nu$	<2%	<2%	7.4%	2.3%	2.2%	<2%
$\frac{1}{2}^-[501]_\nu - \frac{1}{2}^-[501]_\nu$	71.2%	65.7%	24.3%	57.0%	46.9%	2.5%
$\frac{5}{2}^+[633]_\nu - \frac{5}{2}^+[622]_\nu$	<2%	<2%	2.3%	<2%	<2%	<2%
$\frac{13}{2}^+[606]_\nu - \frac{13}{2}^+[606]_\nu$	<2%	<2%	4.3%	<2%	<2%	<2%
$\frac{1}{2}^+[631]_\nu - \frac{1}{2}^+[631]_\nu$	4.7%	10.2%	8.4%	14.5%	22.2%	26.6%
$\frac{5}{2}^+[622]_\nu - \frac{5}{2}^+[622]_\nu$	<2%	<2%	<2%	<2%	8.6%	48.7%
$\frac{5}{2}^-[752]_\nu - \frac{5}{2}^-[752]_\nu$	6.1%	<2%	2.0%	<2%	<2%	<2%
$\frac{7}{2}^-[743]_\nu - \frac{7}{2}^-[743]_\nu$	<2%	10.2%	37.3%	11.3%	7.3%	10.6%

TABLE IV. The same as Table III, but for D_2 pairs.

2-qp basis	^{230}Th	^{232}Th	^{232}U	^{234}U	^{236}U	^{240}Pu
$\frac{3}{2}^-[501]_\nu + \frac{1}{2}^-[501]_\nu$	25.8%	24.7%	26.3%	25.4%	23.5%	<2%
$\frac{5}{2}^-[503]_\nu - \frac{1}{2}^-[501]_\nu$	50.1%	47.6%	52.2%	50.9%	50.1%	<2%
$\frac{3}{2}^+[631]_\nu + \frac{1}{2}^+[631]_\nu$	2.9%	3.3%	3.1%	2.8%	<2%	<2%
$\frac{5}{2}^+[633]_\nu - \frac{1}{2}^+[631]_\nu$	5.4%	7.4%	7.1%	6.3%	2.6%	<2%
$\frac{5}{2}^+[622]_\nu - \frac{1}{2}^+[631]_\nu$	<2%	3.4%	<2%	2.5%	11.6%	98.3%
$\frac{7}{2}^-[743]_\nu - \frac{3}{2}^-[761]_\nu$	2.4%	<2%	<2%	<2%	<2%	<2%
$\frac{3}{2}^+[402]_\pi + \frac{1}{2}^+[400]_\pi$	<2%	2.5%	<2%	<2%	2.1%	<2%

^{240}Pu, the basis $\frac{1}{2}^-[501]_\nu - \frac{1}{2}^-[501]_\nu$ has a very large percentage. Except for ^{230}Th, the configuration $\frac{7}{2}^-[743]_\nu - \frac{7}{2}^-[743]_\nu$ has obvious distributions in the D_0 pairs. The percentages of $\frac{1}{2}^+[631]_\nu - \frac{1}{2}^+[631]_\nu$ and $\frac{5}{2}^+[622]_\nu - \frac{5}{2}^+[622]_\nu$ increase as the neutron number increases due to the shift of the fermi surface. The bases from the proton shell do not play such an important role as those from the neutron shell.

A similar phenomena happens for the structure of D_2 pairs as listed in Table IV. The 2-qp state $\frac{3}{2}^-[501]_\nu + \frac{1}{2}^-[501]_\nu$ has a percentage of about 25% for both ^{230,232}Th and ^{232,234,236}U. For ^{230,232}Th and ^{232,234,236}U, the configuration $\frac{5}{2}^-[503]_\nu - \frac{1}{2}^-[501]_\nu$ plays a very important role with a percentage of about 50%, but less than 2% for ^{240}Pu. The 2-qp configuration $\frac{5}{2}^+[622]_\nu - \frac{1}{2}^+[631]_\nu$ has a percentage of 98.3% for ^{240}Pu and 11.6% for ^{236}U, but very small for the other nuclei. The structure of D_2 pairs agrees well with the results in Ref. [31], where the structures of γ-vibrational states were investigated for rare-earth and actinide-region nuclei by quasiparticle and quasiboson approximation. From Tables III and IV, we see that the D pairs are composed of several 2-qp bases for all the studied nuclei except ^{240}Pu, indicating the collectivity of D pairs we constructed. Although there is only one main component of 2-qp state in D_2 pairs for ^{240}Pu, it is a collective combination of several shell-model sp states.

When one solves Eq. (7), the angular momentum projected energies are then mixed through the diagonalization of the shell model Hamiltonian in Eq. (8). The comparison of the projected energies and the bandhead energies is helpful to identify each band's configuration. As an example, in Fig. 1, we plot the bandhead energies before and after diagonalization for different projected states with $(I^\pi, K^\pi) = (0^+, 0^+)$ and $(I^\pi, K^\pi) = (2^+, 2^+)$ of ^{232}U, respectively. We see from Fig. 1 that both the BCS vacuum state and the D_0 pair have very low energies, while the latter one is about 500 keV higher. After the diagonalization, the ground state becomes nearly 300 keV lower, which indicates that to some extent the vacuum state mixes with the multi-qp states. Similar phenomena happen for the other $K^\pi = 0^+$ states. For the $K^\pi = 2^+$ states, the diagonalization does not make a big difference as that of the$K^\pi = 0^+$ states does. In other words, the $K^\pi = 2^+$ states do not mix so much with each other. The energies of D_0 and D_2 pairs before diagonalization have very little difference with the β- and γ-bandhead energies, respectively. Therefore it can

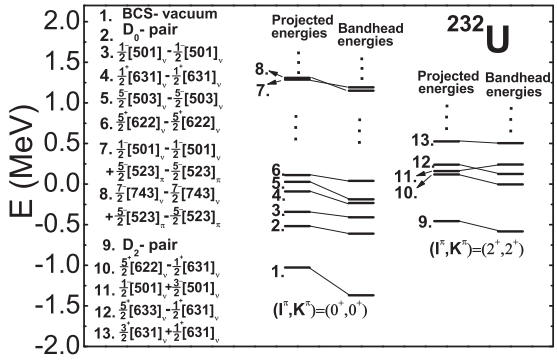

FIG. 1. Comparison of the angular momentum projected energies and the bandhead energies for $(I^\pi, K^\pi) = (0^+, 0^+)$ and $(I^\pi, K^\pi) = (2^+, 2^+)$ states of ^{232}U, respectively. The projected energies represent the values of $H^{I=0}_{0\kappa,0\kappa}/N^{I=0}_{0\kappa,0\kappa}$ and $H^{I=2}_{2\kappa,2\kappa}/N^{I=2}_{2\kappa,2\kappa}$, respectively. The bandhead energies indicate the energies after the diagonalization of Hamiltonian matrix [see Eq. (8)].

be concluded the method to construct the collective pairs as Eq. (1) is very effective.

Based on the collectivity of D pairs, we obtain a more powerful HSM by extending the PSM basis with collective excitations, which is a multishell model and is valid for both qp excitations and low-lying collective excitations such as β and γ vibration. We solve the eigenvalue Eq. (7) in the basis space given by Eq. (4) and get the energy levels and wave functions. Then the $B(E2)$ transitions are calculated by Eq. (14). As a first systemic numerical realization of HSM, we calculate the β and γ bands, some 2-qp and 4-qp rotational bands, and the $B(E2)$ transition rates for ^{230,232}Th, ^{232,234,236}U, and ^{240}Pu, respectively.

For ^{230}Th, we see from Fig. 2 that the ground band agrees well with the experimental data at low spins and has some deviation at spins higher up to $I^\pi = 18^+$. The agreement between the β band and the γ band with the corresponding experimental values is also quite good. Our calculation predicts five 2-qp rotational bands at 985, 1504, 1726, 1661, and 1578 keV with $K^\pi = 0^+$, $K^\pi = 3^+$, $K^\pi =$

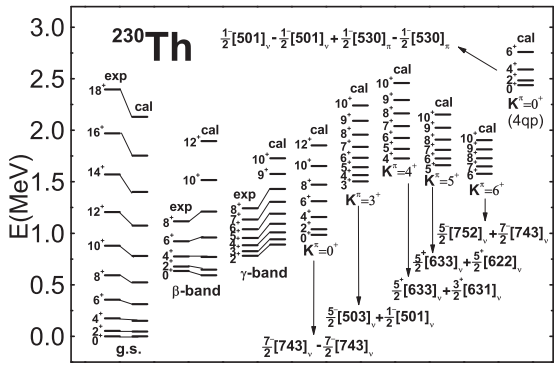

FIG. 2. Comparison of the calculated and experimental g.s. bands, and β and γ bands of ^{230}Th. Some 2-qp and 4-qp rotational bands are also given as a theoretical prediction. The experimental energies are from the National Nuclear Data Center, Ref. [32] and references therein.

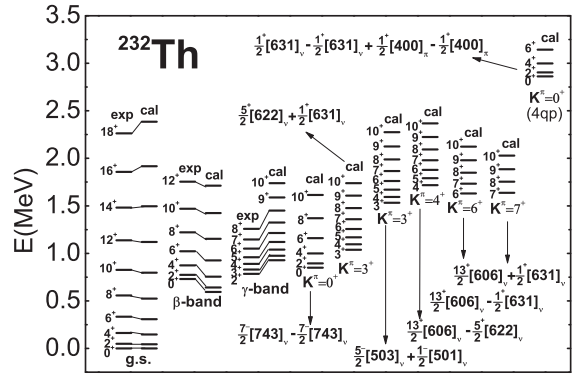

FIG. 3. Same as Fig. 2, but for ^{232}Th.

$4^+, K^\pi = 5^+$, and $K^\pi = 6^+$, respectively. A $K^\pi = 0^+$ 4-qp rotational band is given at 2437 keV with the configuration $\frac{1}{2}^-[501]_\nu - \frac{1}{2}^-[501]_\nu + \frac{1}{2}^-[530]_\pi - \frac{1}{2}^-[530]_\pi$.

In Fig. 3, we plot for ^{232}Th several low-lying multi-qp excited bands and collective bands from HSM and from some available experiment data. We find that the ground band is in good agreement with the experimental values up to spin $I^\pi = 18^+$. The calculated β band is lower than the observed one, obviously, while the case for the γ band is in contrast. The not-very-good reproduction of the γ band may be due to the nonaxial deformation and softness of the realistic potential of this nucleus. It will be discussed at the end of this section. Another $K^\pi = 0^+$ band is predicted at 850 keV with the configuration $\frac{7}{2}^-[743]_\nu - \frac{7}{2}^-[743]_\nu$. Also, there are two $K^\pi = 3^+$ bands at 1037 and 1533 keV with the configuration $\frac{5}{2}^+[622]_\nu + \frac{1}{2}^+[631]_\nu$ and $\frac{5}{2}^-[503]_\nu + \frac{1}{2}^-[501]_\nu$, respectively. At 1718, 1631, and 1640 keV, three bands with $K^\pi = 4^+, K^\pi = 6^+$, and $K^\pi = 7^+$ are predicted, respectively. In our calculation, one 4-qp $K^\pi = 0^+$ rotational band is predicted at 2862 keV, with the configuration $\frac{1}{2}^+[631]_\nu - \frac{1}{2}^+[631]_\nu + \frac{1}{2}^+[400]_\pi - \frac{1}{2}^+[400]_\pi$.

The energy scheme of ^{232}U is given in Fig. 4. We find that the calculation well reproduces the ground band, and β and γ bands. According to the calculation, five 2-qp rotational bands emerge at 960, 1367, 1587, 1481, and 1487 keV with $K^\pi = 0^+$, $K^\pi = 3^+$, $K^\pi = 4^+$, $K^\pi = 6^+$, and $K^\pi = 7^+$, respectively. A low-lying 4-qp rotational band

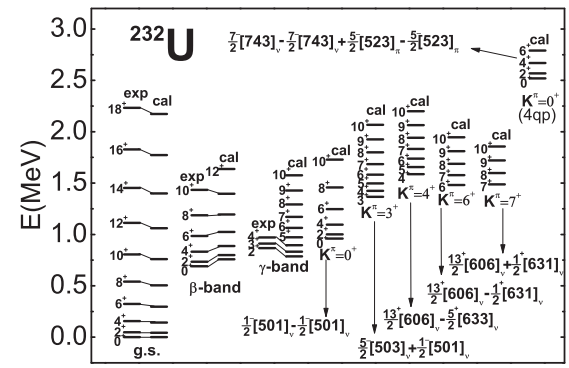

FIG. 4. Same as Fig. 2, but for ^{232}U.

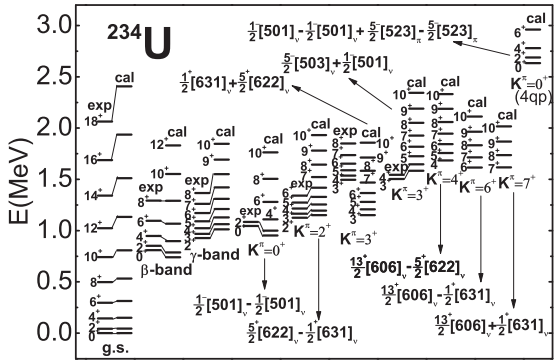

FIG. 5. Same as Fig. 2, but for ^{234}U.

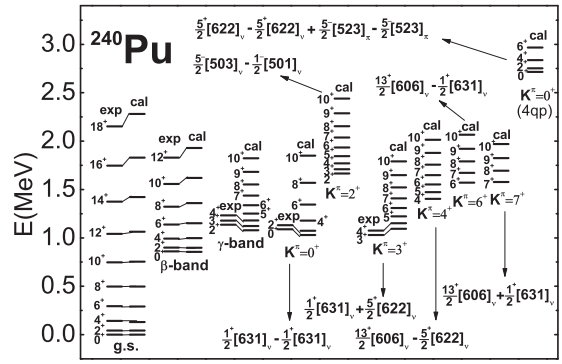

FIG. 7. Same as Fig. 2, but for ^{240}Pu.

with $K^\pi = 0^+$ is predicted at 2520 keV with the configuration $\frac{7}{2}^-[743]_\nu - \frac{7}{2}^-[743]_\nu + \frac{5}{2}^-[523]_\pi - \frac{5}{2}^-[523]_\pi$.

The spectrum is shown in Fig. 5 for ^{234}U. For the ground band, there are visible deviations between the observed values and calculated ones when the spin is larger than 12^+, but at low spin the calculation agrees quite well with experimental data. The calculated β and γ bands at 740 and 1012 keV have some differences, although not large, with the experimental ones which are at 810 and 927 keV, respectively; and moreover, the deviations become larger as the spins increase. A $K^\pi = 0^+$ band with the configuration $\frac{1}{2}^-[501]_\nu - \frac{1}{2}^-[501]_\nu$ is given at 952 keV, and the observed one is at 1044 keV. A $K^\pi = 2^+$ 2-qp band with the configuration $\frac{5}{2}^+[622]_\nu - \frac{1}{2}^+[631]_\nu$ is given at 1150 keV in our calculation, which is nearly the same as the observed value 1125 keV. At 1136 and 1584 keV there are two bands both with $K^\pi = 3^+$ compared with two observed ones at 1496 and 1502 keV, respectively. The $K^\pi = 6^+$ and $K^\pi = 7^+$ bands at 1611 and 1617 keV are also given as a prediction. A $K^\pi = 0^+$ 4-qp rotational band is given at 2633 keV with the configuration $\frac{1}{2}^-[501]_\nu - \frac{1}{2}^-[501]_\nu + \frac{5}{2}^-[523]_\pi - \frac{5}{2}^-[523]_\pi$.

In Fig. 6, the energy scheme for ^{236}U is plotted and compared with the available experimental values. The calculated ground band agrees well with the observed values up to spin $I^\pi = 18^+$. However, the calculated β and γ bands have some deviations, although not large, from the experimental values. A $K^\pi = 0^+$ 2-qp band with configuration

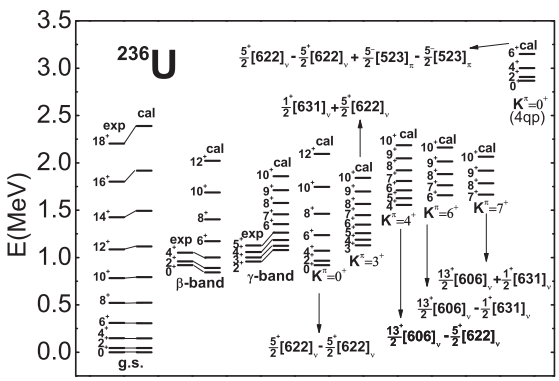

FIG. 6. Same as Fig. 2, but for ^{236}U.

$\frac{5}{2}^+[622]_\nu - \frac{5}{2}^+[622]_\nu$ is plotted at 920 keV as a prediction. Another four 2-qp rotational bands are given at 1129, 1556, 1658, and 1665 keV with $K^\pi = 3^+$, $K^\pi = 4^+$, $K^\pi = 6^+$, and $K^\pi = 7^+$, respectively. A $K^\pi = 0^+$ 4-qp rotational band is given at 2867 keV, with the configuration $\frac{5}{2}^+[622]_\nu - \frac{5}{2}^+[622]_\nu + \frac{5}{2}^-[523]_\pi - \frac{5}{2}^-[523]_\pi$.

The energy scheme of ^{240}Pu is shown in Fig. 7. Both the calculated ground band, β and γ bands, and $K = 3^+$ band agree well with the experimental data. In the calculation, the most important configuration of the γ band is $\frac{5}{2}^+[622]_\nu - \frac{1}{2}^+[631]_\nu$ which is shown in the structure of the D_2 pair in Table IV, and that makes almost no difference with the results of Ref. [31]. The calculation also well reproduces 2-qp rotational bands with $K^\pi = 0^+$ and $K^\pi = 3^+$ at 1029 and 1094 keV compared to the experimental values 1089 and 1031 keV, respectively. Moreover, the configuration of the $K^\pi = 3^+$ band is $\frac{5}{2}^+[622]_\nu + \frac{1}{2}^+[631]_\nu$ in our calculation, which is the same as that suggested in Ref. [32]. Another calculated $K^\pi = 2^+$ band with the configuration $\frac{5}{2}^-[503]_\nu - \frac{1}{2}^-[501]_\nu$ is predicted bandhead energy 1666 keV.

In Ref. [33], ^{240}Pu is studied in the framework of the three-dimensional relativistic Hartree-Bogoliubov calculation with the density-dependent, point-coupling energy density functional, and in the β-γ plane the minimum of binding energy is at the point with $\gamma = 0^\circ$ and $\beta_2 = 0.280$, which indicates the axial symmetry shape. The current HSM is constructed under the assumption of axial symmetry, and the ϵ_2 (0.260) we choose is very close to the shape suggested in Ref. [33].

When the wave functions of the initial and final states are acquired, we calculate the reduced $B(E2)$ transition probabilities between them according to Eq. (14). The interband $B(E2)$ value is a quantity that indicates the K mixing in different bands. In Table V, the calculated intraband $B(E2)$ values of ground bands, and from β and γ bands to ground states are listed and compared with the available observed values in Weisskopf units (W.u.). For the nuclei ^{230}Th, ^{232}U, and ^{240}Pu, the calculated $B(E2)$'s from 2_g^+ to 0_g^+ agree well with the experimental values, while for the other nuclei there exists some difference between the calculation and experimental data, especially for ^{232}Th. For ^{230,232}Th and ^{236}U, the calculated $B(E2)$ transitions from 4_g^+ to 2_g^+ cannot

TABLE V. Comparison of the $B(E2)$ values (in W.u.) between the calculated results and the experimental data. The experimental data are from Ref. [32].

$B(E2)$	^{230}Th		^{232}Th		^{232}U		^{234}U		^{236}U		^{240}Pu	
$I_i \to I_f$	expt.	calc.	expt.	calc.	expt.	calc.	expt.	calc.	expt.	calc.	expt.	calc.
$4_g^+ \to 2_g^+$	265(9)	289.7	286(24)	347.8		376.5		379.6	357(23)	409.3		439.6
$2_g^+ \to 0_g^+$	196(6)	202.0	198(11)	242.7	241(21)	263.1	236(10)	265.0	250(10)	285.8	287(11)	307.3
$2_\beta^+ \to 0_g^+$	2.7(9)	0.37	2.8(12)	0.55		0.64	<1.3	0.54		0.45		0.10
$2_\gamma^+ \to 0_g^+$	2.9(9)	1.27	2.9(4)	1.16		1.32	2.9(5)	1.28		0.56		0.02
$2_\gamma^+ \to 0_\beta^+$		0.10		0.04		1.1		0.01		0.04		0.05

reproduce the experimental data very well. The interband transition probabilities are very small, nearly forbidden. For example, for ^{230,232}Th and ^{234}U the 2_β^+ to 0_g^+ values are 0.37, 0.55, and 0.54 compared to the experimental ones 2.7, 2.8, and 1.3, respectively. Furthermore, for these three nuclei, the experimental $B(E2)$'s from 2_γ^+ to 0_g^+ are all 2.9, but the calculated ones are just 1.27, 1.16, and 1.28, respectively. Therefore, on the whole, the calculated interband transition probabilities are smaller than the experimental data for the transitions from the β or γ band to the ground state. It indicates that in realistic nuclei, the potentials in both β and γ directions are stiffer than those assumed in the HSM, according to the discussion in Ref. [34,35]. The calculated $B(E2)$ transitions from 2_γ^+ to 0_β^+ are also very small.

In the case of the SU(3) limit, according to the FDSM or IBM, the ground state and the degenerated β- and γ-vibrational states belong to different irreducible representations (irrps) of the SU(3) group. The β and γ bands are distinguished by different K values, which means in this case $B(E2)$ transitions between the inter-bands are forbidden. However, both the calculated interband $B(E2)$'s and experimental data are nonzero, which indicates the mixing of the spaces with different irrps.

In Refs. [36,37], the benchmark

$$S(J) = \frac{\{E[J_\gamma^+] - E[(J-1)_\gamma^+]\} - \{E[(J-1)_\gamma^+] - E[(J-2)_\gamma^+]\}}{E[2_g^+]}, \tag{18}$$

is defined to estimate the nonaxiality and softness of the γ deformation. In the equation above, $E[J_\gamma^+]$ is the energy level of γ bands with spin J, and $E[2_g^+]$ is the energy of the first excited state of the ground band. In the case of an axially symmetric rotor, $S(J)$ is equal to 0.333, and the staggering around this value indicates the nonaxial effect. In the microscopic viewpoint, the staggering indicates the mixing of bases with different K^π's [33]. In Fig. 8, we plot the $S(J)$ values of both the observed and calculated γ bands as a function of spin for all the six nuclei we studied. For ^{230}Th, the calculated $S(J)$ values have small deviations from experimental data except at $J^\pi = 9^+$ and 10^+. For ^{234}U, the observed and calculated $S(J)$ values are nearly the same, and moreover, the staggering is still small. According to our calculation, the $S(J)$'s for ^{232}U and ^{240}Pu nearly keep constant at 0.333 at low spins, well reproducing one experimental datum. The calculated $S(J)$'s nearly keep constant at low spins for ^{232}Th. However, the staggering of experimental $S(J)$ data is obvious, indicating the nonaxial shapes of ^{232}Th, and this may explain why the HSM calculation does not well reproduce the experimental γ band for this nucleus. Moreover, for ^{236}U, the staggering of the calculated values is very small, which indicates a good axial shape.

IV. CONCLUSION

In order to describe simultaneously the single-particle and low-lying collective excitations for heavy nuclei, the PSM is extended to the HSM by adding the collective degrees of freedom, namely the D-pairs excitations, into PSM intrinsic basis. The study of the structure of D pairs indicates that the method to construct the D_0 and D_2 pair is reasonable by the linear combination of all the 2-qp states with $K^\pi = 0^+ (K^\pi = 2^+)$ in the PSM truncated space. In this way, the D_0 and D_2 pair does show collectivity.

Based on the collectivity of D pairs, the energy levels and $B(E2)$ transitions for the g.s. band, for 2-qp and 4-qp excitations, and for collective β bands and γ bands are described simultaneously in HSM for deformed actinide nuclei ^{230,232}Th, ^{232,234,236}U, and ^{240}Pu, respectively. The

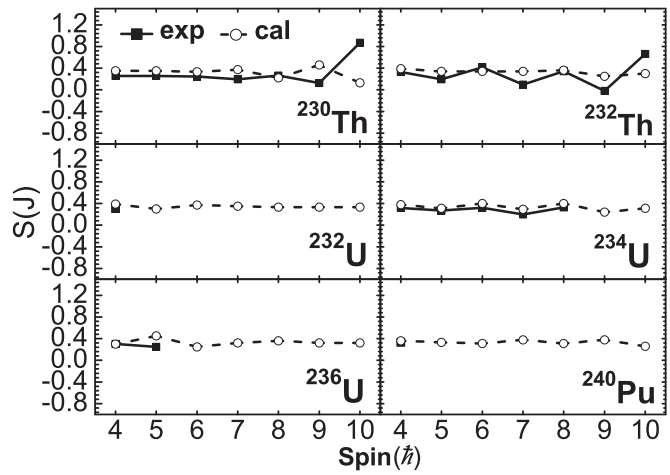

FIG. 8. Comparison of the calculated $S(J)$ values of γ-vibrational bands with experimental data for ^{230,232}Th, ^{232,234,236}U, and ^{240}Pu, respectively.

calculation well reproduces the g.s. bands, β and γ bands, and some quasiparticle bands compared with the observed values, although for ^{232}Th the deviations between the calculated and observed γ bands is big due to the nonaxial deformations. In addition, some low-lying quasiparticle bands are predicted, awaiting experimental confirmation. For all the nuclei studied, the calculated $B(E2)$ values in the g.s. bands from 2_g^+ to 0_g^+ and from 4_g^+ to 2_g^+ and the interband ones agree with the experimental values.

We demonstrate that the HSM can describe simultaneously low-lying collective and quasiparticle excitations in deformed nuclei by adding collective 1-D-pair configurations (D_0 and D_2), and still keep the model space tractable for heavy nuclear systems. HSM could also study 2-phonon excitations by adding 2-D pairs and 2qp-plus-1-D configurations ($a_i^\dagger a_j^\dagger D_K^\dagger|\Phi>$) into the intrinsic basis of PSM, which will be our future work. Along this line, HSM will become a powerful multi-major-shell shell model, useful for both well deformed nuclei and transitional ones.

The symmetry-restoration method discussed in the present paper provides a way to truncate the Hilbert space generally. The method can therefore be applied beyond nuclear physics. In fact, the application of this technique can be found in condensed matter physics [38] and quantum chemistry [39,40], especially for describing electronic states in the Hubbard model [41–44].

ACKNOWLEDGMENTS

Useful discussions with Y.-S. Chen are gratefully acknowledged. This work was supported by the National Natural Science Foundation of China (Grants No. 10975116, No. 11275160, No. 11175258, and No. 11135005) and by the 973 Program of China (No. 2013CB834401).

[1] K. Hara and Y. Sun, Int. J. Mod. Phys. E **04**, 637 (1995).
[2] C.-L. W, D.-H. Feng, and M. Guidry, Adv. Nucl. Phys **21**, 227 (1994).
[3] K. W. Schmid, Prog. Part. Nucl. Phys. **52**, 565 (2004).
[4] Y. Sun, X.-R. Zhou, G. -L. Long, E.-G. Zhao, and P. M. Walker, Phys. Lett. B **589**, 83 (2004).
[5] F. Al-Khudair, G.-L. Long, and Y. Sun, Phys. Rev. C **79**, 034320 (2009).
[6] Y. Sun and M. Guidry, Phys. Rev. C **52**, R2844 (1995).
[7] Y. Sun, J.-y. Zhang, and M. Guidry, Phys. Rev. Lett. **78**, 2321 (1997).
[8] E. Caurier, J.-L. Egido, G. Martinez-Pinedo, A. Poves, J. Retamosa, L.-M. Robledo, and A.-P. Zuker, Phys. Rev. Lett. **75**, 2466 (1995).
[9] K. Hara, Y. Sun, and T. Mizusaki, Phys. Rev. Lett. **83**, 1922 (1999).
[10] G.-L. Long and Y. Sun, Phys. Rev. C **63**, 021305 (2001).
[11] J. A. Sheikh and K. Hara, Phys. Rev. Lett. **82**, 3968 (1999).
[12] J. A. Sheikh, G. H. Bhat, Y.-X. Liu, F.-Q. Chen, and Y. Sun, Phys. Rev. C **84**, 054314 (2011).
[13] F. Iachello and A. Arima, *The Interacting Boson Model* (Cambridge University Press, Cambridge, 1987).
[14] F. Iachello, Phys. Rev. Lett. **53**, 1427 (1984).
[15] Y. Sun, C.-L. Wu, K. Bhatt, M. Guidry, and D.-H. Feng, Phys. Rev. Lett. **80**, 672 (1998).
[16] Y. Sun, C.-L. Wu, K. Bhatt, and M. Guidry, Nucl. Phys. A **703**, 130 (2002).
[17] Y. Sun and C.-L. Wu, Phys. Rev. C **68**, 024315 (2003).
[18] Y. Sun and C.-L. Wu, Int. J. Mod. Phys. E (Suppl.) **17**, 159 (2008).
[19] J.-W. Cui, X.-R. Zhou, F.-Q. Chen, Y. Sun, and C.-L. Wu, Chin. Phys. Lett. **29**, 022101 (2012).
[20] Z.-H. Zhang, J.-Y. Zeng, E.-G. Zhao, and S.-G. Zhou, Phys. Rev. C **83**, 011304(R) (2011).
[21] Z.-H. Zhang, X.-T. He, J.-Y. Zeng, E.-G. Zhao, and S.-G. Zhou, Phys. Rev. C **85**, 014324(R) (2012).
[22] V. Velazquez, J. G. Hirsch, and Y. Sun, Nucl. Phys. A **643**, 39 (1998).
[23] J. Dudek, A. Majhofer, and J. Skalski, J. Phys. G: Nucl. Phys. **6**, 447 (1980).
[24] Z.-C. Gao, Y. Sun, and Y.-S. Chen, Phys. Rev. C **74**, 054303 (2006).
[25] Y.-S. Chen, Y. Sun, and Z.-C. Gao, Phys. Rev. C **77**, 061305 (2008).
[26] S. G. Nilsson *et al.*, Nucl. Phys. A **131**, 1 (1969).
[27] T. Bengtsson and I. Ragnarsson, Nucl. Phys. A **436**, 14 (1985).
[28] J.-P. Delaroche, M. Girod, H. Goutte, and J. Libert, Nucl. Phys. A **771**, 103 (2006).
[29] H. Abusara, A. V. Afanasjev, and P. Ring, Phys. Rev. C **82**, 044303 (2010).
[30] P. Ring and P. Schuck, *The Nuclear Many-Body Problem* (Springer-Verlag, New York, 1980), p. 230.
[31] D. R. Bès, P. Federman, E. Maqueda, and A. Zuker, Nucl. Phys. **65**, 1 (1965).
[32] National Nuclear Data Center, http://www.nndc.bnl.gov/.
[33] Z. P. Li, T. Nikšić, D. Vretenar, P. Ring, and J. Meng, Phys. Rev. C **81**, 064321 (2010).
[34] N. Pietralla and O. M. Gorbachenko, Phys. Rev. C **70**, 011304(R) (2004).
[35] R. F. Casten, *Nuclear Structure from a Simple Perspective* (Oxford University Press, Oxford, 2000), pp. 18–29.
[36] N. V. Zamfir and R. F. Casten, Phys. Lett. B **260**, 265 (1991).
[37] E. A. McCutchan, D. Bonatsos, N. V. Zamfir, and R. F. Casten, Phys. Rev. C **76**, 024306 (2007).
[38] N. Tomita, Phys. Rev. B **69**, 045110 (2004).
[39] C. A. Jiménez-Hoyos, R. Rodriguez-Guzmán, and G. E. Scuseria, J. Chem. Phys. **139**, 204102 (2013).
[40] C. A. Jiménez-Hoyos, R. Rodriguez-Guzmán, and G. E. Scuseria, J. Chem. Phys. **139**, 224110 (2013).
[41] T. Mizusaki and M. Imada, Phys. Rev. B **69**, 125110 (2004).
[42] N. Tomita, Phys. Rev. B **79**, 075113 (2009).
[43] R. Rodriguez-Guzmán, K. W. Schmid, C. A. Jiménez-Hoyos, and G. E. Scuseria, Phys. Rev. B **85**, 245130 (2012).
[44] R. Rodriguez-Guzmán, C. A. Jiménez-Hoyos, R. Schutski, and G. E. Scuseria, Phys. Rev. B **87**, 235129 (2013).